Remote sensing of ocean color: assessment of water-leaving radiance bidirectional effects on atmospheric diffuse transmittance

Haoyu Yang and Howard R. Gordon

Two factors influence the diffuse transmittance (t) of water-leaving radiance (L_w) to the top of the atmosphere: the angular distribution of upwelling radiance beneath the sea surface (L_u) and the concentration and optical properties of aerosols in the atmosphere. We examine these factors and (1) show that the error in L_w that is induced by assuming L_u is uniform (i.e., in treating the subsurface reflectance by the water body as Lambertian) is significant in comparison with the other errors expected in L_w only at low phytoplankton concentration and then only in the blue region of the spectrum; (2) show that when radiance ratios are used in biophysical algorithms the effect of the uniform-L_u approximation is even smaller; and (3) provide an avenue for introducing accurate computation of the uniform-L_u diffuse transmittance into atmospheric correction algorithms. In an Appendix the reciprocity principle is derived for a medium in which the refractive index is a continuous function of position.

1. Introduction

The feasibility of measuring marine phytoplankton concentrations from Earth-orbiting sensors was demonstrated by the proof-of-concept Coastal Zone Color Scanner (CZCS)[1,2] mission. On the basis of the CZCS experience several similar instruments with more spectral bands and higher radiometric sensitivity are being prepared for launch, e.g., the sea-viewing wide field-of-view sensor (SeaWiFS),[3] the moderate-resolution imaging spectroradiometer (MODIS),[4] and so forth. The surrogate for measurement of the phytoplankton concentration is the concentration of the photosynthetic pigment chlorophyll a within the water (actually within the phytoplankton). Because chlorophyll a has a broad, strong absorption in the blue (~435 nm) and a minimum of absorption in the green (~565 nm), the concentration within the water can be estimated from the solar radiance backscattered out of the water near these wavelengths,[5,6] the water-leaving radiance. Unfortunately the water-leaving radiance typically comprises at most 10% of the total radiance that exits the top of the atmosphere (TOA). Briefly the radiance exiting the TOA in a spectral band centered at λ_i, $L_t(\lambda_i)$, can be written

$$L_t(\lambda_i) = L_{\text{other}}(\lambda_i) + L_w{}^a(\lambda_i), \tag{1}$$

where $L_{\text{other}}(\lambda_i)$ represents the contribution to the radiance from all sources except the water-leaving radiance propagated to the TOA, $L_w{}^a(\lambda_i)$. Sources of L_{other} include scattering of solar radiation in the atmosphere, specular reflection of scattered and unscattered radiation from the direct solar beam by the sea surface, and diffuse reflection from oceanic whitecaps. The atmospheric correction algorithm of Gordon and Wang[7,8] estimates L_{other} and removes it from the total radiance, thereby obtaining the water-leaving radiance transmitted to the top of the atmosphere, $L_w{}^a(\lambda_i)$. The water-leaving radiance at the TOA is related to the water-leaving radiance at the bottom of the atmosphere (usually called the water-leaving radiance) through the diffuse transmittance $t(\hat{\xi}_v)$ defined by

$$t(\hat{\xi}_v) \equiv \frac{L_w{}^a(\hat{\xi}_v)}{L_w(\hat{\xi}_v)},$$

where $\hat{\xi}_v$ is a unit vector directed from the sea surface to the sensor and $L_w(\hat{\xi}_v)$ is the water-leaving radiance

The authors are with Department of Physics, University of Miami, P.O. Box 248046, Coral Gables, Florida 33124.

Received 14 November 1996; revised manuscript received 24 April 1997.

0003-6935/97/307887-11$10.00/0

Table 1. Water-Leaving Radiance L_w at 443 and 550 nm as a Function of Pigment Concentration C

C (mg/m^3)	L_w (mW/cm^2 μm sr) 443 nm	550 nm
0.03	1.95–2.20	0.28–0.30
0.10	1.35–1.60	0.28–0.30
0.47	0.40–0.75	0.28–0.40
0.91	0.30–0.50	0.24–0.50

just above the surface. In addition to the attenuation of $L_w(\hat{\xi}_v)$ along the path from the surface to the sensor, the diffuse transmittance also accounts for its augmentation by the scattering of $L_w(\hat{\xi})$ into the direction $\hat{\xi}_v$, i.e., atmospheric scattering from $\hat{\xi}$ to $\hat{\xi}_v$.

The water-leaving radiance L_w can assume a range of values. Table 1 provides values of L_w at 443 and 550 nm with the Sun near the zenith for a range of pigment concentrations C[9] (the sum of the concentrations of chlorophyll a and its degradation product phaeophytin a) for case 1 waters,[5] i.e., waters for which the optical properties are controlled by the water itself, the phytoplankton, and the phytoplankton decay products. The goal of the atmospheric correction algorithm is the derivation of L_w from L_t with an uncertainty of $<5\%$ at 443 nm for very clear oceanic waters, e.g., the Sargasso Sea in summer (for which $C \sim 0.03$ mg/m^3). As t is of the order of unity, the residual error in L_w at 443 nm (after removal of L_{other} from L_t) should be $\lesssim 0.1$ mW/cm^2 μm sr. The Gordon and Wang[7] algorithm is capable of this performance at 443 nm. It is clear that at higher pigment concentrations the relative error in L_w at 443 nm will be higher, e.g., $\sim 25\%$ for $C \sim 1$ mg/m^3 (Table 1). Furthermore the error in the removal of L_{other} at 550 nm is approximately ⅓–¼ that at 443 nm,[10] i.e., ~ 0.03 mW/cm^2 μm sr. Thus even in the Sargasso Sea in summer the relative error in L_w at 550 nm will be $\sim 10\%$.

To retrieve the water-leaving radiance from ${L_w}^a$, we need to calculate the diffuse transmittance. However, as we shall see, the diffuse transmittance itself is a function of the water-leaving radiance, and we generally need to know the angular distribution of the water-leaving radiance to calculate the diffuse transmittance. The angular distribution has been shown to possess significant bidirectional structure[11–13]; however, in the computation of t it has been assumed always that the water-leaving radiance is nearly uniform (independent of viewing direction), i.e., that the deviation of the actual radiance distribution from uniform causes only negligible error in the computation of t. Our objective is to evaluate the validity of this assumption. As we focus on sensors with a spatial resolution of ~ 1 km designed for the open ocean, where the typical scale of variability is a few kilometers, we assume that L_w is constant over the scene. Thus the adjacency effect of the atmosphere[14–16] is ignored. We compare the diffuse transmittance calculated with several realistic water-leaving radiance distributions, including one from actual measurements, with that with a uniform radiance distribution. The results reveal that errors in the retrieved water-leaving radiance caused by making the uniform approximation are significant compared with the error in L_{other} only in the blue and at low pigment concentration.

2. Computational Procedure

For this research we assume the atmosphere is divided into two layers, a molecular-scattering layer on the top and an aerosol layer at the bottom. The ocean surface is assumed to be flat.

The computation of t is straightforward: the radiative transfer equation (RTE) can be solved for the radiance exiting the TOA ${L_w}^a$ with the correct upwelling radiance distribution $L_u(\hat{\xi})$ incident just beneath the sea surface. Accounting for the transfer of radiance across the air–water interface,

$$t(\hat{\xi}) = \frac{{L_w}^a(\hat{\xi})}{L_w(\hat{\xi})},$$

where

$$L_w(\hat{\xi}) = \frac{T_f(\hat{\xi}')}{{m_w}^2} L_u(\hat{\xi}').$$

$T_f(\hat{\xi}')$ is the Fresnel transmittance of the interface for radiance incident from below in the direction $\hat{\xi}'$, and m_w is the refractive index of water. $\hat{\xi}$ and $\hat{\xi}'$ are related by Snell's law. This is the direct approach to finding $t(\hat{\xi})$. However, rather than use this approach we choose to solve the reciprocal problem and use the reciprocity principle (Appendix A) to derive t.

In the reciprocal problem, the extraterrestrial solar beam is incident on the TOA. Let F_0 be the extraterrestrial solar irradiance, $\hat{\xi}_0$ a unit vector in the direction of propagation of the solar beam, and $L_R(\hat{\xi})$ the resulting radiance propagating downward just beneath the sea surface in the direction $\hat{\xi}$. Then it is shown in Appendix A that

$$t(-\hat{\xi}_0) = \frac{1}{F_0|\hat{\xi}_0 \cdot \hat{n}_0| T_f(\hat{\xi}_0)} \int_{\Omega_d} |\hat{\xi} \cdot \hat{n}| L_R(\hat{\xi}) \frac{L_u(-\hat{\xi})}{L_u(-\hat{\xi}_0')} \, d\Omega(\hat{\xi}), \tag{2}$$

where $L_u(-\hat{\xi})$ is the upward radiance distribution incident just beneath the sea surface for which we want t, $\hat{\xi}_0'$ and $\hat{\xi}_0$ are related by Snell's law, and Ω_d indicates the integral is to be evaluated over all downward $\hat{\xi}$. If $L_u(\hat{\xi})$ is uniform, this becomes

$$t^*(-\hat{\xi}_0) = \frac{1}{F_0|\hat{\xi}_0 \cdot \hat{n}_0| T_f(\hat{\xi}_0)} \int_{\Omega_d} |\hat{\xi} \cdot \hat{n}| L_R(\hat{\xi}) d\Omega(\hat{\xi})$$

$$= \frac{E_R(\hat{\xi}_0)}{F_0|\hat{\xi}_0 \cdot \hat{n}_0| T_f(\hat{\xi}_0)}, \tag{3}$$

where $E_R(\hat{\xi}_0)$ is the downward irradiance just beneath the surface in the reciprocal problem.

The relative error in the retrieval of water-leaving

radiance caused in making the uniform radiance approximation is

$$\frac{\Delta L_w(-\hat{\xi}_0)}{L_w(-\hat{\xi}_0)} \equiv \frac{L_w{}^*(-\hat{\xi}_0) - L_w(-\hat{\xi}_0)}{L_w(-\hat{\xi}_0)} = \frac{t(-\hat{\xi}_0) - t^*(-\hat{\xi}_0)}{t^*(-\hat{\xi}_0)}, \quad (4)$$

where $L_w{}^*(-\hat{\xi}_0)$ is computed from $L_w{}^a(-\hat{\xi}_0)$ with $t^*(-\hat{\xi}_0)$. Thus

$$\frac{\Delta L_w(-\hat{\xi}_0)}{L_w(-\hat{\xi}_0)} = \frac{1}{E_R(\hat{\xi}_0)} \int_{\Omega_d} |\hat{\xi} \cdot \hat{n}| L_R(\hat{\xi}) \left[\frac{L_u(-\hat{\xi})}{L_u(-\hat{\xi}_0{}')} - 1 \right] \mathrm{d}\Omega(\hat{\xi}). \quad (5)$$

For the development of the atmospheric correction algorithm, Gordon and Wang[7] carried out extensive simulations (~33,000) of the reciprocal problem for a variety of aerosol models, aerosol optical thicknesses, and $\hat{\xi}_0$. According to Eq. (5) we can use these existing simulations to compute the error for any radiance distribution $L_u(\hat{\xi})$ without having to carry out further radiative transfer simulations. This is the reason for using the reciprocal approach developed here.

3. Computation of the Error in L_w

To compute the error in L_w with Eq. (5), we need the radiance backscattered toward the surface in the water. Precise computation of this requires coupling the ocean and the atmosphere in a multiple-scattering computation. However, because the radiance reflected out of the ocean is small (reflectance <0.04), the probability of photons being reflected out of the ocean twice is negligible. Therefore the coupling is not really required and the ocean and atmosphere can be treated separately.[17] To simplify the computations further we do not consider multiple scattering in the water. Rather we use the quasi-single-scattering approximation (QSSA)[18,19] to provide L_u, given the scattering phase function for the medium. For given optical properties of the ocean the QSSA provides an upwelling radiance distribution beneath the surface that is identical in angular distribution to that produced in single scattering and, as such, represents the upper limit to the departure of L_u from a uniform distribution for a given phase function. The reason for this is that multiple scattering will always produce a radiance distribution smoother than single scattering.

We introduce a Cartesian coordinate system at the sea surface with the z axis pointed in the downward direction (the same direction as $\hat{n}$ at the surface). In this system we describe the direction of $\hat{\xi}$ by the angle θ measured from the z axis and the azimuth angle ϕ measured from the x axis. If $\hat{\xi}$ is directed toward increasing depth, $\theta < 90°$. Thus the direction of the solar beam $\hat{\xi}_0{}'$ in the water is specified by $\theta_0{}'$ and $\phi_0{}'$, and for radiance in the water propagating upward toward the sea surface $\theta > 90°$. We take $\phi_0 = 0$, so photons that are exactly backscattered from the ocean-atmosphere system, i.e., scattered in the direction $-\hat{\xi}_0$, have $\phi = 180°$.

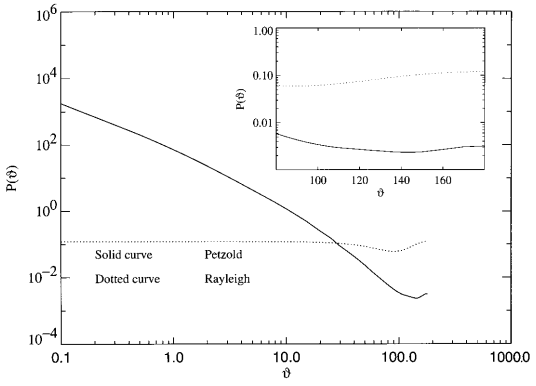

Fig. 1. Comparison of the scattering phase functions for Rayleigh scattering and Petzold's[20] turbid water measurements.

By considering only the refracted direct solar beam in the water, in the QSSA the upwelling radiance distribution just beneath the sea surface is given by[18,19]

$$L_u(\theta, \phi) = C(\omega_0, P) F_0 T(\theta_0) \frac{\cos \theta_0{}' P(\Theta)}{\cos \theta_0{}' - \cos \theta}, \quad (6)$$

where $\cos \theta < 0$ and C is a constant depending mostly on the value of the single-scattering albedo ω_0 but also weakly on P. $P(\Theta)$ is the scattering phase function of the medium for a scattering angle Θ given by

$$\cos \Theta = \cos \theta \cos \theta_0{}' + \sin \theta \sin \theta_0{}' \cos(\phi - \phi_0{}').$$

When diffuse skylight refracted into the water in the direction $\hat{\xi}'$ is considered as well, an additional term

$$C(\omega_0, P) \int_{\hat{\xi}' \cdot \hat{n} > 0} L_d(\hat{\xi}') \frac{\cos \theta' P(\Theta)}{\cos \theta' - \cos \theta} \mathrm{d}\Omega(\hat{\xi}'),$$

where $L_d(\hat{\xi}')$ is the sky radiance transmitted through the air–sea interface and

$$\cos \Theta = \cos \theta \cos \theta' + \sin \theta \sin \theta' \cos(\phi - \phi')$$

must be added to the right-hand side of Eq. (6).

In general the scattering phase function for the ocean, $P(\Theta)$, will be a combination of that attributed to molecular scattering by the water itself (Rayleigh scattering) $P_R(\Theta)$, and that resulting from scattering by the suspended particles $P_p(\Theta)$, i.e.,

$$P(\Theta) = \frac{b_r P_R(\Theta) + b_p P_p(\Theta)}{b_r + b_p},$$

where b_r and b_p are the Rayleigh and particle scattering coefficients, respectively. In contrast to forward-scattering angles for which $P_p(\Theta) \gg P_r(\Theta)$, P_p and P_r are comparable for $\Theta \gtrsim 80°$, so Rayleigh scattering plays an important role in the determination of $P(\Theta)$ for $\Theta \gtrsim 80°$. This is seen in Fig. 1, which compares P_r with P_p measured by Petzold[20] in San Diego harbor. Petzold's San Diego harbor phase

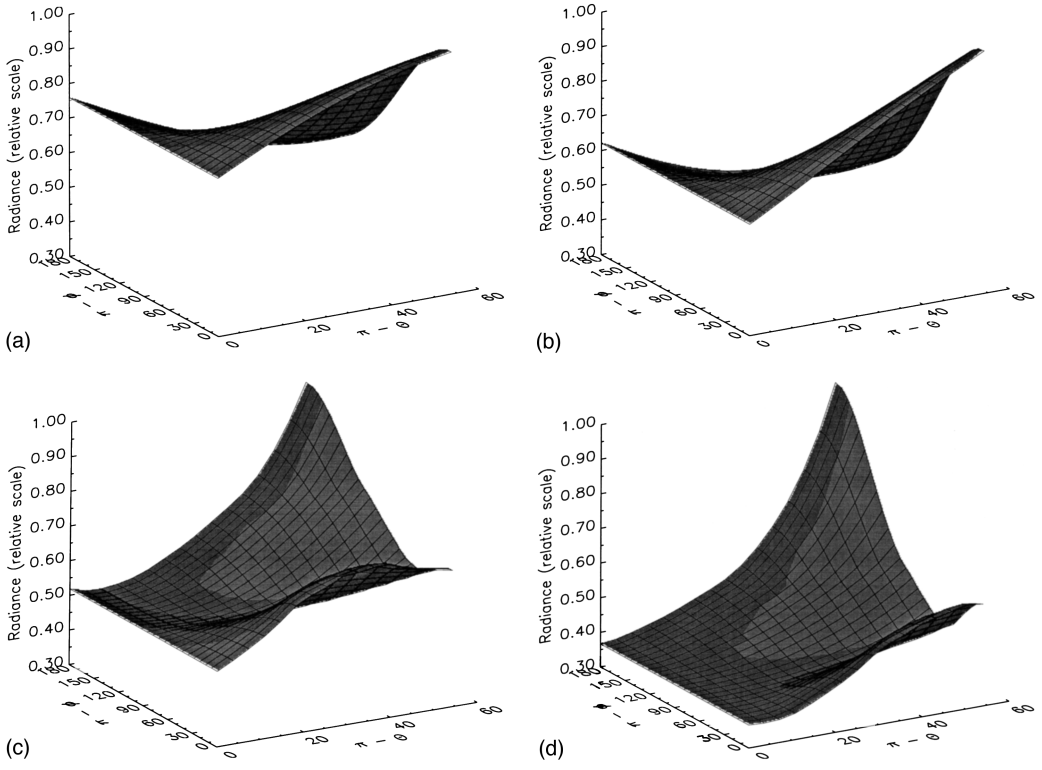

Fig. 2. Subsurface upwelling radiance predicted with the Rayleigh and Petzold phase functions, with radiances normalized to their maximum value: (a) Rayleigh with $\theta_0 = 40°$; (b) Rayleigh with $\theta_0 = 60°$; (c) Petzold with $\theta_0 = 40°$; (d) Petzold with $\theta_0 = 60°$.

function is often taken in ocean radiative transfer simulations as characteristic of particles in ocean water.[21–23]

The limits for $P(\Theta)$ are $P_R(\Theta)(b_p \ll b_r)$ and $P_p(\Theta)(b_p \ll b_r)$. We estimate the error in L_w given by Eq. (5) in these two limits. In general the error falls between these two limits. Figure 2 provides the upward in-water radiance distribution $L_u(-\hat{\xi})$ owing to the direct solar beam alone for these two limits for $\theta_0 = 40°$ and 60°. In Figs. 2(a)–2(d) $\pi - \theta = 0$ implies photons are traveling toward the zenith, and for $\phi = 180°$ ($\pi - \phi = 0$) and $\theta = \theta_0'$ the photons are backscattered exactly. Because photons with $\pi - \theta$ greater than the critical angle (~48°) cannot escape the ocean when the surface is flat, the radiance distributions are truncated at $\pi - \theta = 50°$. Also they are normalized to unity at their maximum value. In the Rayleigh scattering limit an observer looking into the water with $\theta = \theta_0'$ would see maximum radiance for $\phi = 180°$, i.e., with the Sun at the observer's back. In contrast, in the pure particle limit the maximum would be along $\phi = 0$. As we shall see, these radiance distributions lead to different values for the diffuse transmittance t.

We applied Eq. (5) and the QSSA to compute $\Delta L_w/L_w$, the error in the recovered water-leaving radiance made by assuming that $L_u(\theta, \phi)$ is uniform (constant). To compute $L_R(\hat{\xi})$ and $E_R(\hat{\xi}_0)$ in Eq. (5), we assume as in Ref. 7 that the atmosphere can be approximated as two layers with pure molecular scattering in the upper layer and pure aerosol scattering in the lower layer. We use the Shettle and Fenn[24] maritime aerosol model at 90% relative humidity (M90) to provide the aerosol optical properties. The solution of the reciprocal problem was obtained with the successive order-of-scattering method[25] for solving the RTE. The computations are provided for aerosol optical thickness $\tau_a = 0.1$ and 0.2 and wavelengths λ of 443 and 555 nm, the principal spectral regions used to estimate the phytoplankton pigment concentration from L_w.[5] These values for τ_a are typical of those in a pure maritime atmosphere.[26–28]

We begin by examining Sun-viewing geometry typical of scanning ocean color sensors: viewing in the perpendicular plane ($\phi_v = 90°$) at the center of the scan ($\theta_v \approx 0$) and near the scan edge ($\theta_v \approx 45°$), where $\theta_v = 180° - \theta$ and $\phi_v = 180° - \phi$; that is, θ_v is the angle between the direction the radiometer is viewing and the nadir, and photons that backscatter exactly have $\phi_v = 0$. The computations were performed for $\theta_0 = 0°$, 20°, 40°, and 60° and thus cover the sensor's full scan as it progresses along the orbit with ever-increasing solar zenith angles.

Figure 3 provides the error $\Delta L_w/L_w = (t - t^*)/t^*$ by assuming that L_w is uniform. In the case of a pure Rayleigh-scattering ocean [Figs. 3(a) and 3(b)] the maximum error is <1% for all θ_v and θ_0. Furthermore the error depends only weakly on the wavelength and τ_a. In contrast, in the case of a pure particle-scattering ocean [Figs. 3(c) and 3(d)], errors as large as 4% are observed, along with considerable dependence on wavelength and on τ_a. Similar results are obtained in other Sun-viewing geometries. For example, Fig. 4 shows $\Delta L_w/L_w$ as a function of

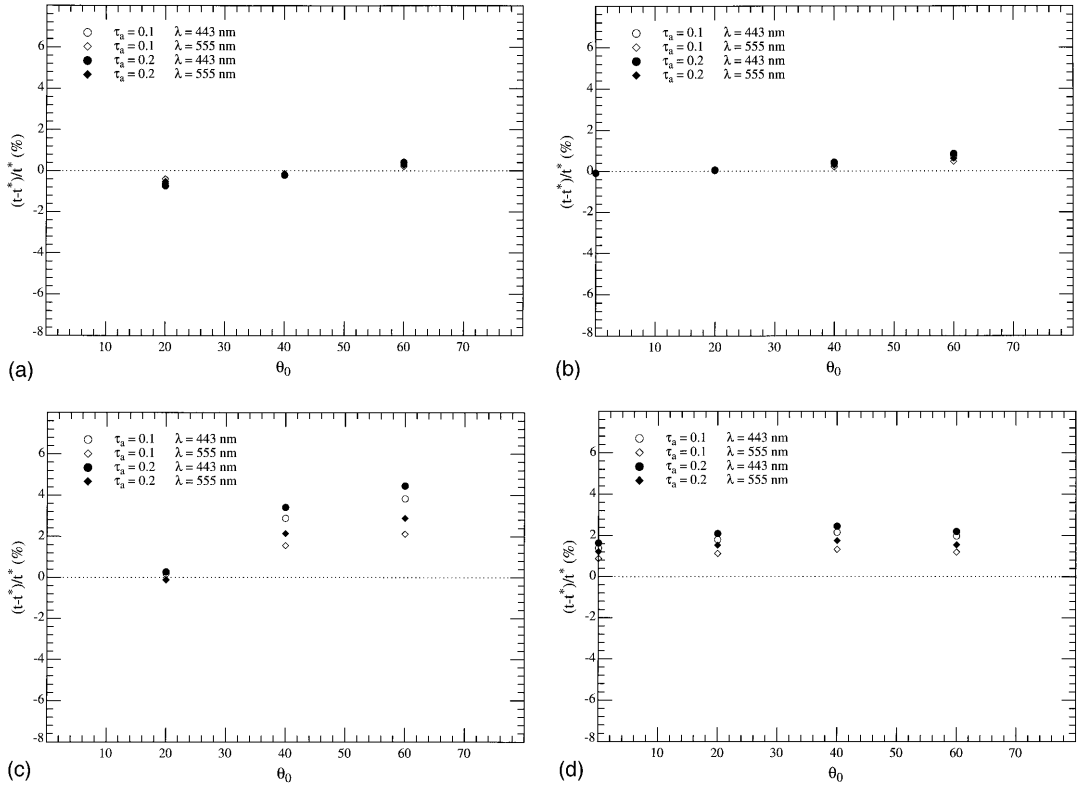

Fig. 3. Error in t, induced by the assumption that L_u is uniform, as a function of wavelength and aerosol optical thickness at the SeaWiFS scan center and scan edge: (a) Rayleigh at the scan center, (b) Rayleigh at the scan edge, (c) Petzold at the scan center, (d) Petzold at the scan edge. Recall that we take the SeaWiFS scan edge to be $\theta_v \approx 45°$. The M90 aerosol model is used in all computations.

the viewing azimuth angle for situations in which $\theta_v = \theta_0$. The resulting errors are similar to those in Fig. 3 although, in the case of a Rayleigh-scattering ocean, the error near $\phi_v = 0$ or 180° (the principal plane) is much greater than that near $\phi_v = 90°$ (the perpendicular plane). As most ocean color instruments scan closer to the perpendicular plane than to the principal plane, this is not considered important. Figure 5 provides the error as a function of the viewing angle in the perpendicular plane. The behavior is similar to that in Fig. 4 although the error does not exceed 4% over the meaningful range of θ_v (0°–60°).

These results can be explained qualitatively by the variation of $L_u(\theta, \phi)$ in the vicinity of the observation direction. In Eq. (5) $L_R(\hat{\xi})$, the radiance propagating downward just beneath the sea surface when the source is the solar beam incident on the TOA in the direction $\hat{\xi}_0$, is strongly peaked near $\hat{\xi} = \hat{\xi}_0'$. This causes the error $(t - t^*)/t^*$ to be largely governed by the behavior of $L_u(-\hat{\xi})$ in directions near $-\hat{\xi}_0'$. Thus $(t - t^*)/t^*$ will be positive if $L_u(-\hat{\xi})$ near the observation direction $(-\hat{\xi}_0')$ is larger than $L_u(-\hat{\xi}_0')$; that is, if we are observing in the direction of a relative minimum in $L_u(-\hat{\xi})$, $(t - t^*)/t^* > 0$. Conversely when observing near a local maximum in $L_u(-\hat{\xi})$, $(t - t^*)/t^* < 0$. Consider Fig. 4(d); as ϕ_v varies with $\theta_v = \theta_0$, the observation point moves parallel to the $\pi - \theta$ axis along $\pi - \theta = 40.5°$ in Fig. 2(d). For $\phi_v = 0$, $L_u(\theta_v', \phi_v)$ is a maximum, and with increasing ϕ_v a minimum is reached near $\theta_v = 60°$ and a second maximum is reached at $\phi_v = 180°$. As expected, Fig. 4(d) shows the inverse pattern in $(t - t^*)/t^*$. A similar pattern is seen in Fig. 4(c) compared with Fig. 2(c); however, in Fig. 2(c) the L_u minimum is near $\phi_v = 90°$ rather than 60° and the maximum at $\phi_v = 180°$ is not as strong. Figures 4(a) and 4(b) show a pattern contrasting with Figs. 4(c) and 4(d) in that the maximum in $(t - t^*)/t^*$ occurs at $\phi_v = 180°$. This is attributed to the fact that for the Rayleigh-scattering case the maximum in the L_u surface for a given θ_v occurs at $\phi_v = 0$, and the radiance then decreases monotonically to a minimum at $\phi_v = 180°$. The maximum values of $|(t - t^*)/t^*|$ are approximately the same for the two water-scattering phase functions in Fig. 4, but this should be expected as the range of variation of L_u is similar in all four cases examined.

The small $(t - t^*)/t^*$ values in the principal plane for the Rayleigh-scattering case [Figs. 3(a) and 3(b)] are now easy to understand: as ϕ_v varies near 90°, positive and negative contributions to the integral in Eq. (5) from smaller values of ϕ_v are canceled by contributions from larger values. The results in Fig. 5 can be explained in a similar manner.

The dependence of $(t - t^*)/t^*$ on λ and τ_a in Figs. 5(a)–5(d) is caused by their effect on $L_R(\hat{\xi})$ in Eq. (5). As τ_a increases or λ decreases, the sky radiance becomes more diffuse and the contributions to the integral in Eq. (5) can come from directions $-\hat{\xi}$ farther from $-\hat{\xi}_0'$. Because most of the sky radiance in directions far from $\hat{\xi}_0$ is attributed to Rayleigh scatter-

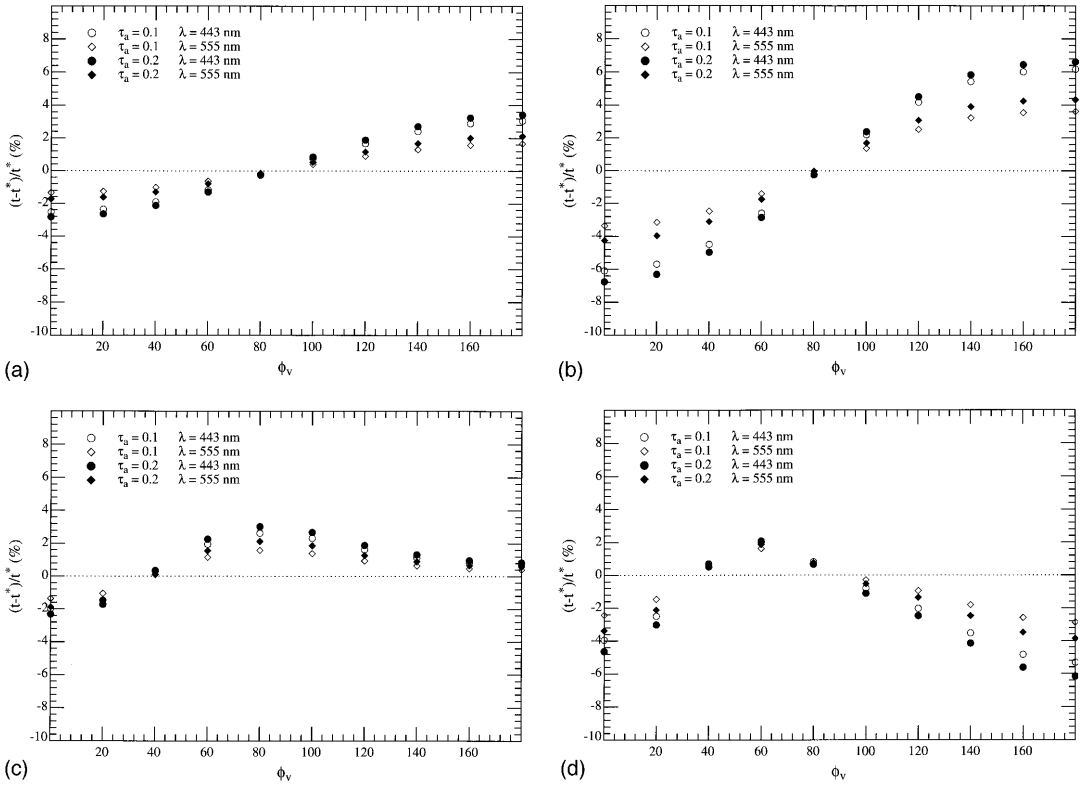

Fig. 4. Error in t, induced by the assumption that L_u is uniform, as a function of wavelength, aerosol optical thickness, and viewing azimuth ϕ_v for $\theta_0 = \theta_v$: (a) Rayleigh with $\theta_0 = 40°$, (b) Rayleigh with $\theta_0 = 60°$, (c) Petzold with $\theta_0 = 40°$, (d) Petzold with $\theta_0 = 60°$. The M90 aerosol model is used in all computations.

ing, changing from 555 to 443 nm, which increases the Rayleigh-scattering optical thickness τ_r by a factor of ~2.5, causes a much greater change in the magnitude of $(t - t^*)/t^*$ than doubling the aerosol optical thickness. Also as expected, the magnitude of $(t - t^*)/t^*$ is greater in the blue than in the green for all cases we examined.

We also carried out computations of $\Delta L_w/L_w$ using actual measurements of radiance distributions made by Voss[13,29] on the R/V *New Horizon* west of San Diego at 32°40′N and 121°18′W. In this case the water itself contributed ≲1–2% to the total backscattering in the blue.[13] The radiance distributions at 450 and 500 nm are provided in Fig. 6 for $\theta_0 = 60°$. Note the similarity of these to those for the particle-dominated ocean [Figs. 2(c) and 2(d)]; however, the total variation (minimum to maximum) of the measured $L_u(\theta, \phi)$ is smaller, as would be expected in the presence of multiple scattering. Figure 7 provides the resulting $\Delta L_w/L_w$ as a function of ϕ_v with $\theta_v = \theta_0$ [Fig. 7(a)] and as a function of θ_v in the perpendicular plane [Fig. 7(b)] for 443 and 510 nm. For the 443-nm computations L_u at 450 nm was used, while for 510 nm L_u at 500 nm was used. The resulting errors are similar to those provided in Figs. 4 and 5. The strikingly different behavior of the error at the two wavelengths for $\phi_v = 0$ and 60° in Fig. 7(b) is explained by the differences in the two radiance distributions.

By considering that the goal of atmospheric correction is recovering L_w at 443 nm to within ±5% in very clear ocean water, we see that the assumption that $L_u(\theta, \phi)$ is uniform can lead to significant error in L_w in such situations, i.e., errors in magnitude similar to L_{other}, when the phase function is similar to Petzold's[20] or when the radiance distribution is similar to that measured on the *New Horizon*. However, in more productive waters or in the green the error in the recovered L_w induced by this assumption will usually be small compared with that induced by error in removing L_{other}, that is, the error in ${L_w}^a$ itself will be considerably more than the error in L_w induced by replacing t by t^*.

Finally most algorithms for relating L_w to water constituents involve the use of radiance ratios.[5] For algorithms that make use of the ratio $L_w(443)/L_w(555)$, e.g., the CZCS phytoplankton pigment algorithm, Figs. 3–5 suggest that the error in this ratio induced by replacing t by t^* is ≲2%, with the exception of a very clear ocean (Rayleigh scattering) viewing near $\phi_v = 0$ with $\theta_v = \theta_0 = 60°$, for which the error is ~3% [Fig. 4(b)].

4. Inclusion of *t** in Atmospheric Correction

It is clear that usually t can be replaced by t^*, so it is important to include accurate computation of t^* in the atmospheric correction algorithm. Equation (3) shows that t^* is simply the transmittance of solar irradiance from the TOA to just beneath the sea surface. This quantity is easily computed,[30]

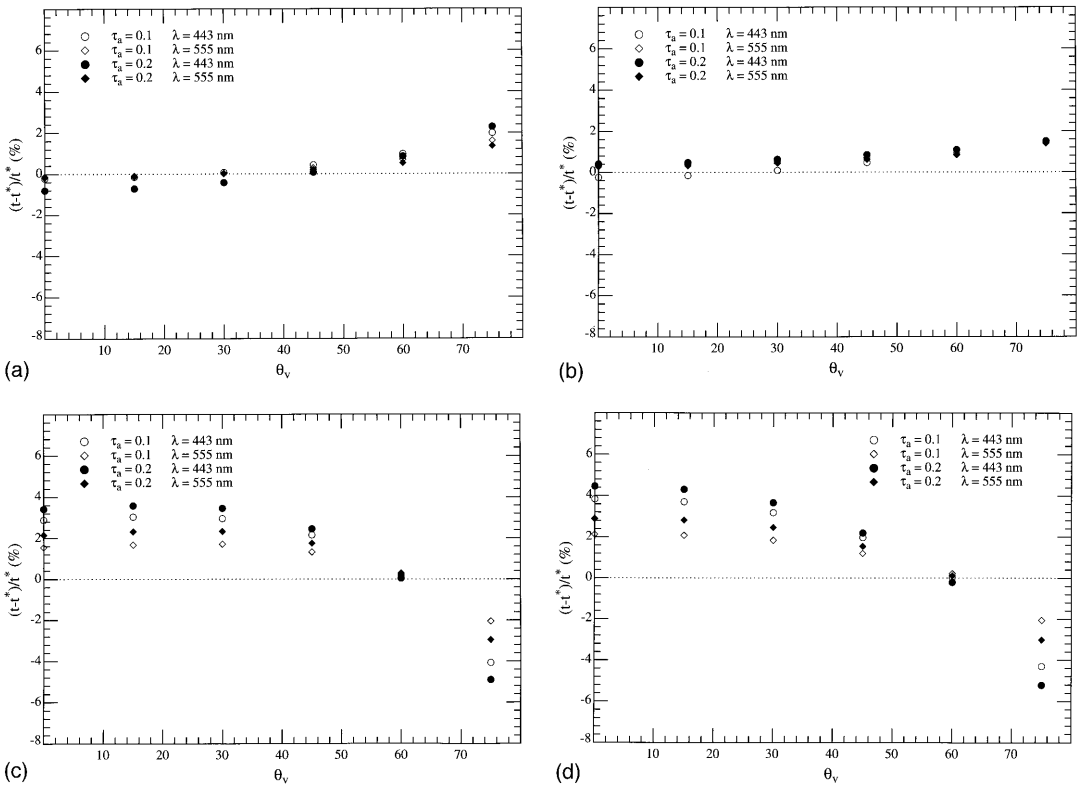

Fig. 5. Error in t, induced by the assumption that L_u is uniform, as a function of wavelength, aerosol optical thickness, and viewing angle θ_v in the perpendicular plane of the Sun: (a) Rayleigh with $\theta_0 = 40°$, (b) Rayleigh with $\theta_0 = 60°$, (c) Petzold with $\theta_0 = 40°$, (d) Petzold with $\theta_0 = 60°$. Recall that for SeaWiFS we take the scan edge to be $\theta_v \approx 45°$. The M90 aerosol model is used in all computations.

and studies[6,14] show that because of the strong forward scattering associated with aerosols, if the aerosol is nonabsorbing, t^* is only a weak function of the aerosol optical thickness τ_a. Furthermore additional simulations we carried out (not shown) demonstrate that as expected, when the aerosol is absorbing, t^* is independent of the aerosol vertical structure.

In the original CZCS atmospheric correction algorithm the presence of aerosol was ignored completely and t^* was approximated simply as $\exp(-\tau_r/2 \cos \theta_v)$.[6,14] We propose a simple method of including accurate computation of t^* in the Gordon and Wang[7,10] atmospheric correction algorithm. Recall that the Gordon and Wang algorithm makes use of the variation of L_{other} in the near infrared (NIR) to select an aerosol model from a set of candidate models for estimating L_{other} in the visible. After an aerosol model is chosen, L_{other} in the NIR can be used to estimate τ_a at all wavelengths. An aerosol model and τ_a are all that are needed to compute t^* accurately. Our simulations show that for a given aerosol model the dependence of t^* on τ_a is almost exponential; that is, $t^*(\theta) \approx A(\theta)\exp[-B(\theta)\tau_a]$. Thus for a given θ only two precomputed parameters are needed to provide t^*. For effecting the removal of L_{other}, a set of lookup tables (LUT's) were prepared that relate L_{other} to τ_a for each candidate aerosol model, Sun-viewing geometry, and wavelength by solving the RTE for a two-

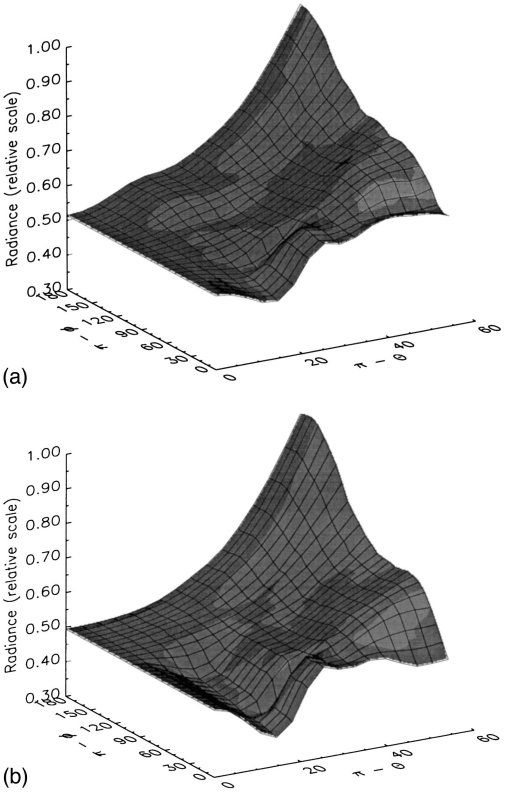

Fig. 6. Subsurface upwelling radiance distributions measured by Voss with the radiance distribution system (RADS)[13,29]: (a) λ = 450 nm, $\theta_0 = 58.2°$; (b) λ = 500 nm, $\theta_0 = 59.7°$.

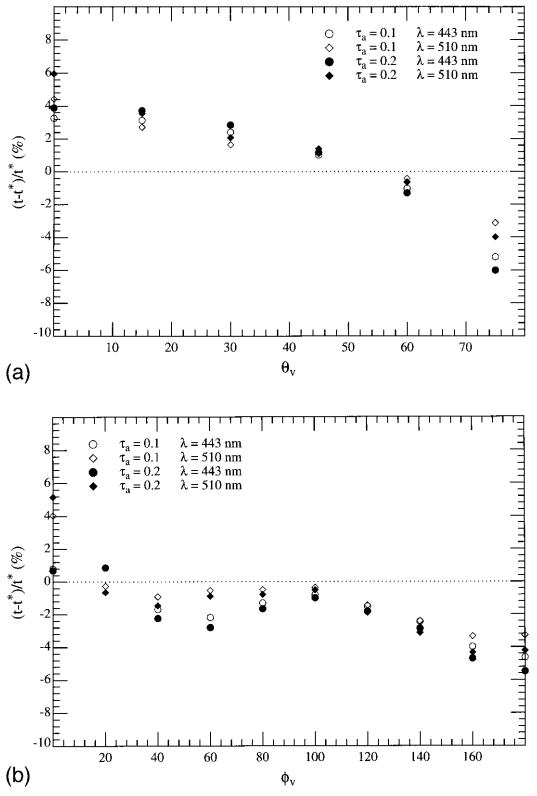

Fig. 7. Error in t, induced by the assumption that L_u is uniform, as a function of wavelength and aerosol optical thickness, with the Voss subsurface upwelling radiance distribution: (a) $\theta_0 = 60°$ viewing in the perpendicular plane to the Sun, (b) $\theta_v = \theta_0 = 60°$ with viewing azimuth ϕ_v. The M90 aerosol model is used in all computations.

layer atmosphere (aerosols on the bottom). These existing solutions to the RTE can be used with Eq. (3) for computing the required t^* because t^* does not depend on the vertical structure of the aerosol. Because the L_{other} LUT's were prepared for $\theta_0 = 0(2.5°)80°$, i.e., 33 values of θ_0, LUT's that relate t^* to τ_a with the same resolution require only 66 constants for each wavelength and candidate aerosol model of interest. In contrast the LUT's for L_{other} require $\sim$35,000 constants per aerosol model per wavelength. Thus computation of a precise value of $t^*(\theta)$ within the framework of the Gordon and Wang algorithm is not a challenge.

5. Concluding Remarks

We examine the effects of factors that influence the diffuse transmittance of the water-leaving radiance to the top of the atmosphere: the angular distribution of upwelling radiance beneath the sea surface and the concentration and optical properties of the aerosol in the atmosphere. Several conclusions are possible based on the analysis.

First, the error in L_w that is made by assuming that L_u is uniform is $\lesssim$4% for viewing geometries typical of ocean color observations and aerosol optical thicknesses typical of the open-ocean marine atmosphere. Because the error in retrieving ${L_w}^a$ from L_t will usually exceed 4% by a considerable amount, the departure of L_u from uniform usually can be ignored. An exception is for low values of C in the blue where ${L_w}^a$ is large and its removal from L_t can be expected to be in error by $\lesssim$5%. Thus for atmospheric correction over clear water in the blue it will be necessary to estimate the angular distribution of L_u in the computation of t to insure that the error in L_w remains $<$5%. This can be accomplished with an estimate of C, obtained with t^*, in an iterative manner as suggested by Morel and Gentili.[31] In contrast, for sensors that are capable of viewing over a large range of azimuth angles, e.g., the polarization and directionality of the Earth reflectance instrument (POLDER mission),[32] the uniform L_u assumption can lead to an error of more than 6% in L_w (Fig. 4), and the error is highly dependent on the viewing azimuth relative to the Sun. Second, when biophysical products, e.g., C, are derived from ratios of L_w at two wavelengths, the effect of replacing t by t^* is significantly smaller than the effect on L_w. Finally, accurate computation of t^* can be included in any atmospheric correction algorithm that makes use of candidate aerosol models to remove L_{other}, e.g., Ref. 7.

Appendix A: Reciprocity Principle

Case[33] and Case and Zweifel[34] provide a generalization of Chandrasekhar's[35] derivation of the reciprocity principle. However, both Case's and Chandrasekhar's results are applicable only to media with a constant index of refraction. Because we were unable to find in the literature a similar result for media with variable refractive index, we provide here a derivation of the reciprocity principle for a medium in which the refractive index m is a function of position. We then use this to derive Eq. (2).

In the absence of internal sources with such a medium occupying a volume V and illuminated from the outside, the radiance $L(\ell, \hat{\xi})$ along a ray is governed by the RTE,

$$\frac{\mathrm{d}}{\mathrm{d}\ell}\left[\frac{L(\ell,\hat{\xi})}{m^2(\ell)}\right] = -c(\ell)\frac{L(\ell,\hat{\xi})}{m^2(\ell)} + \int_{4\pi}\beta(\ell;\hat{\xi}'\to\hat{\xi})\frac{L(\ell,\hat{\xi})}{m^2(\ell)}\,\mathrm{d}\Omega(\hat{\xi}'), \quad \text{(A1)}$$

where $\hat{\xi}$ is a unit vector tangent to the path of the ray and ℓ is measured along the ray. In this equation $\beta(\ell;\hat{\xi}'\to\hat{\xi})$ is the volume-scattering function for scattering from $\hat{\xi}'$ to $\hat{\xi}$, $c(\ell)$ is the beam attenuation coefficient of the medium, and $\mathrm{d}\Omega(\hat{\xi}')$ is a differential of solid angle around $\hat{\xi}'$. To derive the reciprocity principle we imagine a given medium with two different radiance distributions incident on a volume V from the outside. We index the solution to these two

problems by indices 1 and 2. Thus for problem 1 we have

$$\frac{\mathrm{d}}{\mathrm{d}\ell}\left[\frac{L_1(\ell,\hat{\xi})}{m^2(\ell)}\right] = -c(\ell)\frac{L_1(\ell,\hat{\xi})}{m^2(\ell)} + \int_{4\pi}\beta(\ell;\hat{\xi}'\to\hat{\xi})\frac{L_1(\ell,\hat{\xi}')}{m^2(\ell)}\,\mathrm{d}\Omega(\hat{\xi}'), \tag{A2}$$

with a similar equation for problem 2. Now in problem 2 we reverse the sign of $\hat{\xi}$ everywhere, i.e.,

$$-\frac{\mathrm{d}}{\mathrm{d}\ell}\left[\frac{L_2(\ell,-\hat{\xi})}{m^2(\ell)}\right] = -c(\ell)\frac{L_2(\ell,-\hat{\xi})}{m^2(\ell)} + \int_{4\pi}\beta(\ell;\hat{\xi}'\to-\hat{\xi})\frac{L_2(\ell,\hat{\xi}')}{m^2(\ell)}\,\mathrm{d}\Omega(\hat{\xi}'), \tag{A3}$$

where the minus sign on the left-hand side is introduced so that the direction of increasing ℓ is in the direction $+\hat{\xi}$ in both problems 1 and 2. The integral term in Eq. (A3) can be rearranged in the following manner: first, because the direction $\hat{\xi}'$ is an integration variable, it can be replaced by $-\hat{\xi}'$ everywhere in the integral; next we recall that $\beta(\ell;-\hat{\xi}'\to-\hat{\xi}) = \beta(\ell;\hat{\xi}\to\hat{\xi}')$; and finally we note that $\mathrm{d}\Omega(-\hat{\xi}') = \mathrm{d}\Omega(\hat{\xi}')$. Thus the integral term in Eq. (A3) can be written

$$\int_{4\pi}\beta(\ell;\hat{\xi}\to\hat{\xi}')\frac{L_2(\ell,-\hat{\xi}')}{m^2(\ell)}\,\mathrm{d}\Omega(\hat{\xi}').$$

Now multiply Eq. (A2) by $L_2(\ell,-\hat{\xi})/m^2(\ell)$ and Eq. (A3) by $L_1(\ell,\hat{\xi})/m^2(\ell)$ and subtract. Then multiply the result by $m^2(\ell)\mathrm{d}\Omega(\hat{\xi})\mathrm{d}V$ and integrate over all $\Omega(\hat{\xi})$ and over V. The left-hand side of the result is

$$\int_{4\pi}\mathrm{d}\Omega(\hat{\xi})\int_V m^2(\ell)\frac{\mathrm{d}}{\mathrm{d}\ell}\left[\frac{L_1(\ell,\hat{\xi})}{m^2(\ell)}\frac{L_2(\ell,-\hat{\xi})}{m^2(\ell)}\right]\mathrm{d}V,$$

and the right-hand side is

$$\int_V\mathrm{d}V\int\mathrm{d}\Omega(\hat{\xi})m^2(\ell)\int\beta(\ell;\hat{\xi}'\to\hat{\xi})\frac{L_1(\ell,\hat{\xi}')}{m^2(\ell)}\frac{L_2(\ell,-\hat{\xi})}{m^2(\ell)}\times\mathrm{d}\Omega(\hat{\xi}') - \int_V\mathrm{d}V\int\mathrm{d}\Omega(\hat{\xi})m^2(\ell)\times\int\beta(\ell;\hat{\xi}\to\hat{\xi}')\frac{L_1(\ell,\hat{\xi})}{m^2(\ell)}\frac{L_2(\ell,-\hat{\xi}')}{m^2(\ell)}\,\mathrm{d}\Omega(\hat{\xi}').$$

Clearly the terms on the right-hand side add to zero, so

$$\int_{4\pi}\mathrm{d}\Omega(\hat{\xi})\int_V m^2(\ell)\frac{\mathrm{d}}{\mathrm{d}\ell}\left[\frac{L_1(\ell,\hat{\xi})}{m^2(\ell)}\frac{L_2(\ell,-\hat{\xi})}{m^2(\ell)}\right]\mathrm{d}V = 0$$

Now we write $\mathrm{d}V = \mathrm{d}A(\hat{\xi})\mathrm{d}\ell$, where $\mathrm{d}A(\hat{\xi})$ is a differential of area with normal in the direction of $\hat{\xi}$. Then with the fact that $m^2(\ell)\mathrm{d}A(\hat{\xi})\mathrm{d}\Omega(\hat{\xi})$ is constant along the path of the ray,[36]

$$\int_{\ell_1}^{\ell_2}\frac{\mathrm{d}}{\mathrm{d}\ell}\left[\int_A\int_{4\pi}\frac{L_1(\ell,\hat{\xi})}{m^2(\ell)}\frac{L_2(\ell,-\hat{\xi})}{m^2(\ell)}m^2(\ell)\mathrm{d}\Omega(\hat{\xi})\mathrm{d}A(\hat{\xi})\right]\times\mathrm{d}\ell = 0,$$

or

$$\int_A\int_{4\pi}\left[\frac{L_1(\ell,\hat{\xi})L_2(\ell,-\hat{\xi})}{m^2(\ell)}\,\mathrm{d}\Omega(\hat{\xi})\mathrm{d}A(\hat{\xi})\right]_{\ell_1}^{\ell_2} = 0,$$

where ℓ_1 is the beginning of the path in V (the position where the ray enters V) and ℓ_2 is the end of the path (the position where the ray exits V). If $\hat{n}$ is the outward normal to the surface of V, $\mathrm{d}A(\hat{\xi})$ at ℓ_1 or ℓ_2 is $\hat{\xi}\cdot\hat{n}\mathrm{d}S$, where $\mathrm{d}S$ is the associated differential element of area on the surface of V, and this equation becomes

$$\int_S\mathrm{d}S\int_{4\pi}\hat{\xi}\cdot\hat{n}\,\frac{L_1(\boldsymbol{\rho},\hat{\xi})L_2(\boldsymbol{\rho},-\hat{\xi})}{m^2(\boldsymbol{\rho})}\,\mathrm{d}\Omega(\hat{\xi}) = 0, \tag{A4}$$

with $\boldsymbol{\rho}$ specifying the position of a point on the surface. This is the reciprocity principle for a medium with variable m. It can be rearranged to read

$$\int_S\mathrm{d}S\int_{\hat{\xi}\cdot\hat{n}<0}|\hat{\xi}\cdot\hat{n}|\left[\frac{L_1(\boldsymbol{\rho},\hat{\xi})L_2(\boldsymbol{\rho},-\hat{\xi})}{m^2(\boldsymbol{\rho})} - \frac{L_1(\boldsymbol{\rho},-\hat{\xi})L_2(\boldsymbol{\rho},\hat{\xi})}{m^2(\boldsymbol{\rho})}\right]\mathrm{d}\Omega(\hat{\xi}) = 0, \tag{A5}$$

where the integration over $\Omega(\hat{\xi})$ is only over directions for which $\hat{\xi}\cdot\hat{n}<0$. When there are internal sources in the medium of intensity density, $Q(\mathbf{r},\hat{\xi})$, where $\mathbf{r}$ specifies the position of a point in the medium, a term $Q(\mathbf{r},\hat{\xi})/m^2(\mathbf{r})$ must be added to the right-hand side of Eq. (A1). In this case it is easy to show that the right-hand side of Eq. (A5) becomes

$$\int_{4\pi}\mathrm{d}\Omega(\hat{\xi})\int_V\mathrm{d}V\left[\frac{Q_2(\mathbf{r},-\hat{\xi})L_1(\mathbf{r},\hat{\xi})}{m^2(\mathbf{r})} - \frac{Q_1(\mathbf{r},\hat{\xi})L_2(\mathbf{r},-\hat{\xi})}{m^2(\mathbf{r})}\right].$$

It is straightforward to use this to derive Eq. (2). Consider a volume with upper surface at the top of the atmosphere and lower surface just beneath the sea surface. Then for problem 1 choose the incident radiance on the TOA to be that of the solar beam; that is, $L_1(\boldsymbol{\rho}_T,\hat{\xi}) = F_0\delta(\hat{\xi}-\hat{\xi}_0)$, where $\boldsymbol{\rho}_T$ is a TOA point and $\hat{\xi}_0$ is the direction of the solar beam. We assume that there is no upward radiance incident at $\boldsymbol{\rho}_B$, a point just beneath the sea surface; that is, $L_1(\boldsymbol{\rho}_B,\hat{\xi}) = 0$ for $\hat{\xi}\cdot\hat{n}<0$. This is referred to in the text as the reciprocal problem. For problem 2 (the direct problem in the text) we let $L_2(\boldsymbol{\rho}_T,\hat{\xi}) = 0$ for $\hat{\xi}\cdot\hat{n}<0$ (no incident radiance on the TOA) and $L_2(\boldsymbol{\rho}_B,\hat{\xi})$ be spec-

ified for $\hat{\xi} \cdot \hat{n} < 0$, i.e., a specified upward radiance distribution incident on the bottom surface. Then, applying Eq. (A5), we have

$$L_2(\boldsymbol{\rho}_T, -\hat{\xi}_0) = \frac{1}{F_0|\hat{\xi}_0 \cdot \hat{n}|} \int_{\Omega_d} |\hat{\xi} \cdot \hat{n}| \times \frac{L_1(\boldsymbol{\rho}_B, \hat{\xi}) L_2(\boldsymbol{\rho}_B, -\hat{\xi})}{m_w^2} \, d\Omega(\hat{\xi}),$$

where Ω_d is the full solid angle in the downward direction and m_w is the refractive index of water. Letting $\hat{\xi}_0'$ be the direction of the refracted solar beam in the water for a flat surface,

$$\frac{L_2(\boldsymbol{\rho}_T, -\hat{\xi}_0)}{L_2(\boldsymbol{\rho}_B, -\hat{\xi}_0')} = \frac{1}{F_0|\hat{\xi}_0 \cdot \hat{n}| m_w^2} \int_{\Omega_d} |\hat{\xi} \cdot \hat{n}| \times L_1(\boldsymbol{\rho}_B, \hat{\xi}) \frac{L_2(\boldsymbol{\rho}_B, -\hat{\xi})}{L_2(\boldsymbol{\rho}_B, -\hat{\xi}_0')} \, d\Omega(\hat{\xi}). \quad \text{(A6)}$$

In the absence of absorption and scattering in the atmosphere,

$$L_1(\boldsymbol{\rho}_B, \hat{\xi}) = T_f(\hat{\xi}_0) F_0 \frac{|\hat{\xi}_0 \cdot \hat{n}|}{|\hat{\xi}_0' \cdot \hat{n}|} \delta(\hat{\xi} - \hat{\xi}_0'),$$

where $T_f(\hat{\xi})$ is the Fresnel transmittance of the interface. Equation (A6) then yields

$$L_2(\boldsymbol{\rho}_T, -\hat{\xi}_0) = \frac{T_f(\hat{\xi}_0)}{m_w^2} L_2(\boldsymbol{\rho}_B, -\hat{\xi}_0'),$$

which is the familiar relationship for the propagation of radiance across the air–sea interface. If we replace $L_2(\boldsymbol{\rho}_B, -\hat{\xi}_0')$ in Eq. (A6) by $L_w(\boldsymbol{\rho}_B, -\hat{\xi}_0)$, the water-leaving radiance just above the sea surface; that is,

$$L_2(\boldsymbol{\rho}_B, -\hat{\xi}_0') = \frac{m_w^2}{T_f(\hat{\xi}_0)} L_w(\boldsymbol{\rho}_B, -\hat{\xi}_0),$$

then Eq. (A6) becomes

$$\frac{L_2(\boldsymbol{\rho}_T, -\hat{\xi}_0)}{L_w(\boldsymbol{\rho}_B, -\hat{\xi}_0)} = \frac{1}{F_0|\hat{\xi}_0 \cdot \hat{n}| T_f(\hat{\xi}_0)} \int_{\Omega_d} |\hat{\xi} \cdot \hat{n}| \times L_1(\boldsymbol{\rho}_B, \hat{\xi}) \frac{L_2(\boldsymbol{\rho}_B, -\hat{\xi})}{L_2(\boldsymbol{\rho}_B, -\hat{\xi}_0')} \, d\Omega(\hat{\xi}) \equiv t(-\hat{\xi}_0).$$

$t(-\hat{\xi}_0)$ is the quantity we defined as the diffuse transmittance in Eq. (2).

The authors gratefully acknowledge the National Aeronautics and Space Administration for support under grant NAGW-273 and contracts NAS5-31363 and NAS5-31734. They also thank K. J. Voss for kindly providing the radiance distribution data used in Fig. 6.

References

1. W. A. Hovis, D. K. Clark, F. Anderson, R. W. Austin, W. H. Wilson, E. T. Baker, D. Ball, H. R. Gordon, J. L. Mueller, S. Y. E. Sayed, B. Strum, R. C. Wrigley, and C. S. Yentsch, "Nimbus 7 coastal zone color scanner: system description and initial imagery," Science **210k** 60–63 (1980).
2. H. R. Gordon, D. K. Clark, J. L. Mueller, and W. A. Hovis, "Phytoplankton pigments derived from the Nimbus-7 CZCS: initial comparisons with surface measurements," Science **210,** 63–66 (1980).
3. S. B. Hooker, W. E. Esaias, G. C. Feldman, W. W. Gregg, and C. R. McClain, "An overview of SeaWiFS and ocean color," Technical Memorandum 104566 in Technical Report Series, Vol. 1, 1992 (NASA, Greenbelt, Md.).
4. V. V. Salomonson, W. L. Barnes, P. W. Maymon, H. E. Montgomery, and H. Ostrow, "MODIS: advanced facility instrument for studies of the Earth as a system," IEEE Trans. Geosci. Remote Sens. **27,** 145–152 (1989).
5. H. R. Gordon and A. Y. Morel, *Remote Assessment of Ocean Color for Interpretation of Satellite Visible Imagery: A Review* (Springer-Verlag, New York, 1983).
6. H. R. Gordon, D. K. Clark, J. W. Brown, O. B. Brown, R. H. Evans, and W. W. Broenkow, "Phytoplankton pigment concentrations in the Middle Atlantic Bight: comparison between ship determinations and Coastal Zone Color Scanner estimates," Appl. Opt. **22,** 20–36 (1983).
7. H. R. Gordon and M. Wang, "Retrieval of water-leaving radiance and aerosol optical thickness over the oceans with SeaWiFS: a preliminary algorithm," Appl. Opt. **33,** 443–452 (1994).
8. H. R. Gordon and M. Wang, "Influence of oceanic whitecaps on atmospheric correction of SeaWiFS," Appl. Opt. **33,** 7754–7763 (1994).
9. H. R. Gordon, O. B. Brown, R. H. Evans, J. W. Brown, R. C. Smith, K. S. Baker, and D. K. Clark, "A semi-analytic radiance model of ocean color," J. Geophys. Res. **93D,** 10,909–10,924 (1988).
10. H. R. Gordon, "Atmospheric correction of ocean color imagery in the Earth Observing System era," *J. Geophys. Res.* **102D,** 17,081–17,106 (1997).
11. A. Morel and B. Gentili, "Diffuse reflectance of oceanic waters: its dependence on Sun angle as influenced by the molecular scattering contribution," Appl. Opt. **30,** 4427–4438 (1991).
12. A. Morel and B. Gentili, "Diffuse reflectance of oceanic waters. II: bidirectional aspects," Appl. Opt. **32,** 6864–6879 (1993).
13. A. Morel, K. J. Voss, and B. Gentili, "Bidirectional reflectance of oceanic waters: a comparison of modeled and measured upward radiance fields," J. Geophys. Res. **100C,** 13,143–13,150 (1995).
14. D. Tanre, M. Herman, P. Y. Deschamps, and A. de Leffe, "Atmospheric modeling for space measurements of ground reflectances, including bidirectional properties," Appl. Opt. **18,** 3587–3594 (1979).
15. Y. J. Kaufman, "Atmospheric effect on spatial resolution of surface imagery," Appl. Opt. **23,** 3400–3408 (1984).
16. P. Reinersman and K. L. Carder, "Monte Carlo simulation of the atmospheric point-spread function with an application to correction of the adjacency effect," Appl. Opt. **34,** 4453–4471 (1995).
17. H. R. Gordon, "Radiative transfer: a technique for simulating the ocean in satellite remote sensing calculations," Appl. Opt. **15,** 1974–1979 (1976).
18. H. R. Gordon, "Simple calculation of the diffuse reflectance of the ocean," Appl. Opt. **12,** 2803–2804 (1973).
19. H. R. Gordon, "Modeling and simulating radiative transfer in the ocean," in *Ocean Optics*, R. W. Spinrad, K. L. Carder, and M. J. Perry, eds. (Oxford U. Press, New York, 1994), pp. 3–39.
20. T. J. Petzold, "Volume scattering functions for selected natural waters," SIO Ref. No. 72-78, 1972 (Scripps Institution of Oceanography, Visibility Laboratory, San Diego, Calif. 92152).
21. J. T. O. Kirk, "Estimation of the scattering coefficient of nat-

ural waters using underwater irradiance measurements," Aust. J. Mar. Freshwater Res. **32,** 533–539 (1981).
22. J. T. O. Kirk, "The upwelling light stream in natural waters," Limnol. Oceanogr. **34,** 1410–1425 (1989).
23. J. T. O. Kirk, "Estimation of the absorption and scattering coefficients of natural waters by the use of underwater irradiance measurements," Appl. Opt. **33,** 3276–3278 (1994).
24. E. P. Shettle and R. W. Fenn, "Models for the aerosols of the lower atmosphere and the effects of humidity variations on their optical properties," Report AFGL-TR-79-0214, 1979 (Air Force Geophysics Laboratory, Hanscomb AFB, Mass.).
25. H. C. van de Hulst, *Multiple Light Scattering* (Academic, New York, 1980).
26. P. J. Reddy, F. W. Kreiner, J. J. Deluisi, and Y. Kim, "Aerosol optical depths over the Atlantic derived from shipboard sunphotometer observations during the 1988 Global Change Expedition," Global Biogeochem. Cycles **4,** 225–240 (1990).
27. G. K. Korotaev, S. M. Sakerin, A. M. Ignatov, L. L. Stowe, and E. P. McClain, "Sunphotometer observations of aerosol optical thickness over the North Atlantic from a Soviet research vessel for validation of satellite measurements," J. Atmos. Oceanic Technol. **10,** 725–735 (1993).
28. Y. V. Villevalde, A. V. Smirnov, N. T. O'Neill, S. P. Smyshlyaev, and V. V. Yakovlev, "Measurement of aerosol optical depth in the Pacific Ocean and North Atlantic," J. Geophys. Res. **99D,** 20,983–20,988 (1994).
29. K. J. Voss, "Electro-optic camera system for measurement of the underwater radiance distribution," Opt. Eng. **28,** 241–247 (1989).
30. K. N. Liou, *Radiation and Cloud Processes in the Atmosphere* (Oxford U. Press, New York, 1992).
31. A. Morel and B. Gentili, "Diffuse reflectance of oceanic waters. III: implication of bidirectionality for the remote sensing problem," Appl. Opt. **35,** 4850–4862 (1996).
32. P. Y. Deschamps, F. M. Bréon, M. Leroy, A. Podaire, A. Bricaud, J. C. Buriez, and G. Sèze, "The POLDER mission: instrument characteristics and scientific objectives," IEEE Trans. Geosci. Remote Sens. **32,** 598–615 (1994).
33. K. M. Case, "Transfer problems and the reciprocity principle," Rev. Mod. Phys. **29,** 651–663 (1957).
34. K. M. Case and P. F. Zweifel, *Linear Transport Theory* (Addison-Wesley, Reading, Mass., 1967).
35. S. Chandrasekhar, *Radiative Transfer* (Oxford U. Press, Oxford, UK, 1950).
36. W. T. Welford, *Aberrations in Optical Systems* (Hilger, Bristol, UK, 1986).